Vietnam Journal of Science and Technology ***64***(2) (2026) 328–340
DOI: https://doi.org/10.15625/2525-2518/19492

High efficiency of Ag-g-C_3N_4@HAp as green catalyst for photodegradation of tetracycline

Pham Xuan Nui*, Pham Thi Yen Phi, Phan Trung Kien

Department of Chemical Engineering, Hanoi University of Mining and Geology, 18 Vien street, Dong Ngac ward, Ha Noi, Viet Nam

*Email: *phamxuannui@humg.edu.vn*

Received: 25 November 2023; Accepted for publication: 29 February 2024

Abstract. In the present work, a green method was used for the synthesis of Ag-g-C_3N_4@HAp nanocomposite. Namely, hydroxyapatite (HAp) and silver nanoparticles (Ag-NPs) were synthesized using biological waste and natural materials as seashells and *Centella asiatica* (L.) Urban extract. The structure, morphology and composition of the composites were characterized by XRD, SEM and EDX methods. Besides, TEM images showed that silver nanoparticles dispersed on g-C_3N_4 and HAp. XPS spectra determined the valence state of elements in the composite. The superior optical properties of g-C_3N_4@HAp containing Ag-NPs with low band gap energy (Eg = 2.59 eV) demonstrated degradation of tetracycline up to 99.5 % compared to HAp pure (90 %) and g-C_3N_4@HAp (96 %). Ag-g-C_3N_4@HAp nanocomposite has potential as a green photocatalyst for the removal of industrial wastewater pollutants.

Keywords: HAp, g-C_3N_4, tetracycline (TC), Ag-g-C_3N_4@HAp, composite.

Classification numbers: 3.3.3, 3.4.2, 3.7.3.

1. INTRODUCTION

In recent years, two-dimensional (2D) layered graphical carbon nitride (g-C_3N_4) nanosheets have been known as photocatalyst materials due to their adjustable electronic structure, good thermal stability and chemical stability, narrow bandgap energy (2.7 eV), non-toxicity and eco-friendly material [1-4]. However, due to the limited specific surface area, low visible light utilization efficiency, and rapid recombination of photo-generated electron-hole pairs, which limits the widespread application of g-C_3N_4 [5]. To overcome the disadvantages of the single g-C_3N_4 photocatalyst design, composite photocatalysts based on g-C_3N_4 have been studied to improve the photocatalytic efficiency. For example, some noble metals (Pt, Au or Ag) have been deposited on g-C_3N_4 to enhance the photocatalytic activity of g-C_3N_4 [6, 7]. Among them, silver nanoparticles (Ag NPs) have received much more attention due to its lower cost. Patnaik *et al.* [8] used Ag/g-C_3N_4 for degradation of organic pollutants and water splitting. Bu *et al.* [9] synthesized Ag-modified mesoporous g-C_3N_4 using a photoassisted reduction method. Ag nanoparticles (Ag-NPs) were fabricated by a $NaBH_4$ reduction method to decorate g-C_3N_4 sheet photocatalyst [10]. Recently, silver nanoparticles have been synthesized from leaf extracts of *Polyalthia longifolia, Geranium (Pelargonium graveolens), Eucalyptus citriodora (neelagiri), Ficus benghalensis (marri)* and *Centella asiatica* (L.) [11, 12]. Among them, the *Centella*

asiatica (L.) is a herb with high medicinal values, its antioxidant properties and non-toxicity, which have used as a raw material source to synthesize Ag-NPs [13].

Besides, Fina *et al.* [14] reported loading Pt nanoparticles on g-C_3N_4 to improve the activity of g-C_3N_4 for H_2 production from water. Manimozhi *et al.* [15] designed heterojunction of ZnO/g-C_3N_4 photocatalyst for degradation of organic dyes.

In addition, hydroxyapatite ($Ca_{10}(PO_4)_6(OH)_2$) is an inorganic material that has been widely used in the biomedical field. This is because of some of there unique properties including biological activity, biocompatibility, and non-toxicity. On another hand, the HAp has a high specific surface area, low solubility in water, mechanical stability and thermal stability makes it an excellent green adsorbent and ion exchanger for the removal of hazardous dye molecules [16-21]. The HAp has been synthesized from natural sources such as eggshells, seashells, animal bone, etc. using different methods including wet-chemical, sol-gel, microwave, hydrothermal and electrochemical deposition, etc. [22].

In general, the HAp does not decompose organic dyes under visible light irradiation due to its large band gap energy [23]. Many studies have been conducted using g-C_3N_4 for modification of HAp material. For example, Xu *et al.* [24] synthesized a novel and stable g-C_3N_4/HAp composites as highly efficient photocatalysts for rapid degradation of tetracycline. Ehiro [25] fabricated g-C_3N_4/HAp from urea and animal bone by calcination method. Mantilla *et al.* [26] synthesized a new g-C_3N_4/HAp photocatalyst composite using precipitation and thermal condensation methods and its application for the photoreduction of Cr(VI) under UV and visible light irradiation. Beygli *et al.* [27] used g-C_3N_4 modified with hydroxyapatite to adsorb metal ions from wastewater. Along with the rapid development of industry, in the field of medicine, the presence of antibiotics in water has caused concern in modern life. Among antibiotics, tetracycline (TC) is commonly used and discharged directly into water environment, causing adverse effects on human health and ecosystem equilibrium.

Based on the above issues, here we developed seashell and *Centella asiatica* (L.) Urban extract to synthesize a green photocatalyst Ag-g-C_3N_4@HAp with photocatalytic stability and high catalytic performance for removal of tetracycline under visible light irradiation. The experimental results demonstrated that seashells derived Z-Scheme Ag-g-C_3N_4@HAp composite can be a promising photocatalyst for degradation and removal of TC in wastewater.

2. EXPERIMENTALS

2.1. Materials

Silver nitrate ($AgNO_3$, ≥ 99.0 %), urea ($(NH_2)_2CO$, 99.0 %), sodium hydroxide (NaOH, ≥ 98.0 %), di-ammonium hydrogen phosphate ($(NH_4)_2HPO_4$, ≥ 98.0 %), poly vinyl alcohol (PVA, 99.0%), ethanol (C_2H_5OH, ~96.0 %), tetracycline (TC, 98.0 %). All of these chemicals were purchased from Sigma-Aldrich and used without further purification. Seashells were heated 990 °C for 3 h to obtain CaO powder, silver nanoparticles were fabricated from *Centella asiatica* (L.) Urban extract according to previous study [26, 28].

2.2. Synthesis of hydroxyapatite (HAp)

HAp was synthesized according to the following procedure: The seashells ($CaCO_3$) were collected from the sea beach of the coastal town of Quang Ninh province, Viet Nam. These shells

were cleaned, deproteinized and heated at about 900 °C to obtain CaO according to the reaction equation:

$$CaCO_3 \xrightarrow{900\,^{\circ}C} CaO + CO_2 \quad (1)$$

The above CaO (2.6 g) was dissolved in the distilled water (50 mL) with continuous stirring to obtain a homogeneous suspension. 0.3 M solution of $(NH_4)_2HPO_4$ was slowly added to the suspension solution. The molar ratio of Ca/P was 0.7. This solution was then continuously stirred for 2 h at room temperature, maintaining the pH of the solution at 10 (adjustment using 1 M NaOH solution). The suspension was then crystallized in an autoclave at 180 °C for 24 h. The precipitate was washed several times with distilled water and dried overnight at 120 °C to obtain the HAp powders.

2.3. Synthesis of Ag-g-C_3N_4@HAp composite

g-C_3N_4@HAp composite was synthesized through condensation process. The synthesized HAp (0.5 g) was mixed with urea (6.25 g) by manual grinding in agate mortar and the mixture was then placed in a ceramic crucible and heated at 500 °C for 2 h (10 °C/min). Finally, the yellow powders obtained as g-C_3N_4@HAp composite. For comparation, the g-C_3N_4 pure was synthesized by grinding 6.25 grams of urea in agate mortar and heating at 500 °C for 2 h (10 °C/min).

Ag-NPs synthesis process from *Centella asiatica* (L.) Urban extract was performed according to our previous study [29]. In brief, 100 grams of leaves were washed and dried at room temperature, then ground and extracted using the Soxhlet system with an 80/20 (v/v) ratio of deionized water and ethanol. The extract was obtained by evaporation of ethanol. 20 mL of 0.01 M $AgNO_3$ solution was slowly added to the extract and continuously stirred at 40°C for 1 h to obtain Ag-NPs.

10 mL of *Centella Asiatica* (L.) aqueous extract containing silver nanoparticles was added into 0.1 g of g-C_3N_4@HAp composite. The mixture was subjected to ultrasound for 30 min. The product was filtered, washed with distilled water and dried overnight at 90 °C to obtain the Ag (0.05 wt.%)-g-C_3N_4 (1.0 wt.%)@HAp composite and was denoted in this work as Ag-g-C_3N_4@HAp.

2.4. Characterization

The phase structure of materials was determined by X-ray diffraction (XRD) using a D-8 Advance with a Cu K_α source ($\lambda = 0.154$ nm). The composition and oxidation state of the elements were determined by energy-dispersive X-ray (EDX) and X-ray photoelectron spectroscopy (XPS). The optical properties of materials were evaluated through UV-vis using a HITACHI U-3900 spectrophotometer. The morphology of materials was studied by scanning electron microscopy (SEM) using a JEOL JSM 6390 LV and transmission electron microscopy (TEM) techniques using a Leica IEO 906E.

2.5. Photocatalytic activity test

The photocatalytic activity of composite was evaluated through degradation of tetracycline. In the photocatalytic model reaction, 40 mg of Ag-g-C_3N_4@HAp photocatalyst was dispersed in a 50 mL TC aqueous solution (50–90 ppm). This reaction system was irradiated by visible light using a 100 W Xe lamp as the light source. Before the photocatalytic reactions were carried out,

the solution was stirred magnetically in the dark for 30 min to achieve adsorption equilibrium. The photocatalytic reaction was then conducted with time intervals, 4 mL of the suspension was extracted and centrifuged, and the supernatant was analyzed by UV-vis spectrophotometer at a wavelength of 357 nm to determine the TC concentration. The degradation efficiency (DE) of TC was determined using Eq. (1).

$$DE(\%) = \frac{C_0 - C_t}{C_0} \times 100 \quad (2)$$

where C_o và C_t are the initial concentration and concentration at various time intervals of TC, respectively.

3. RESULTS AND DISCUSSION

3.1. Characteristics of materials

The crystalline phase structure of the samples was determined by X-ray diffraction technique. Figure 1(a) shows a strong diffraction peak at 2-theta=27.5° corresponding to the reflection plane of (200) with hexagonal unit cell lattice in pure g–C_3N_4 sample (JCPDS Card No.87–1526). The XRD pattern of g-C_3N_4@HAp composite (Figure 1(b)) matches with polycrystalline structure of HAp and g-C_3N_4, namely, diffraction peaks at 2θ = 25.8°, 28.9°, 31.6°, 33°, 46.5°, 49.5° and 54.7° are assigned to diffraction planes (002), (102), (311), (300), (222), (213) and (004) of HAp (JCPDS Card No. 09–0432) [26, 30], and (200) of g-C_3H_4. Besides, the XRD pattern of Ag-g-C_3N_4@HAp composite (Figure 1(c)) shows the appearance of peaks at 2θ = 38.4° and 44.2°. These peaks are assigned to the (111), (200) crystalline plane of metallic Ag, respectively (JCPDS 04-0783) [31]. This indicates that the Ag-g-C_3N_4@HAp composite photocatalyst was successfully synthesized in this study.

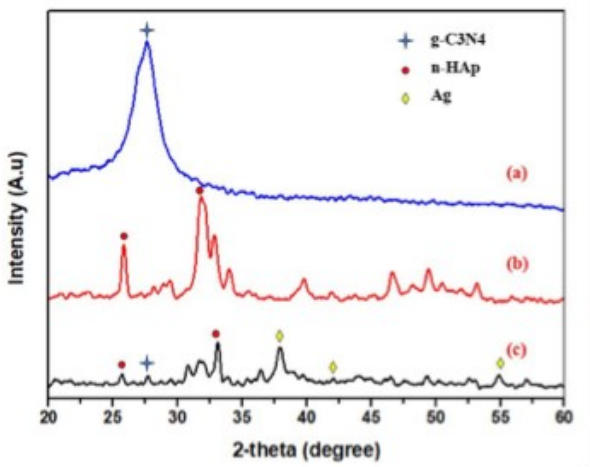

Figure 1. XRD diffraction of (a) g-C_3N_4, (b) g-C_3N_4@HAp, and (c) Ag-g-C_3N_4@HAp.

In addition, the chemical composition of the synthesized Ag-g-C_3N_4@HAp composite was analyzed through EDX (Figure 2(a)) and elemental mapping images (Figure 2(b)) analysis. The elemental mapping images of composite demonstrate the existence of all elements including C, N, O, P, Ca and Ag in the composite.

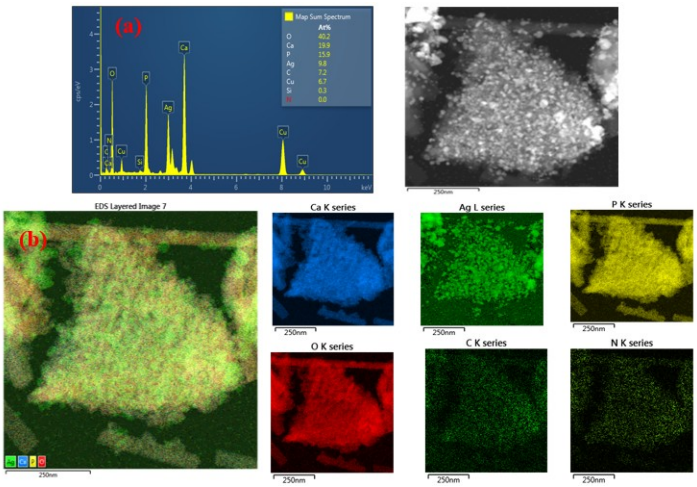

Figure 2. (a) EDX spectra and (b) elemental mapping images of Ag-g-C_3N_4@HAp composite.

The morphology of the synthesized samples was characterized by SEM and TEM techniques. Figure 3(a) shows the ultrafine sheets of g-C_3N_4 and the uniform agglomerates of HAp (Figure 3(b)). The SEM images of g-C_3N_4@HAp composite shows that sphere–shaped nanoparticles of HAp implanted on the surface of g-C_3N_4 sheets (Figures 3(c), (d)).

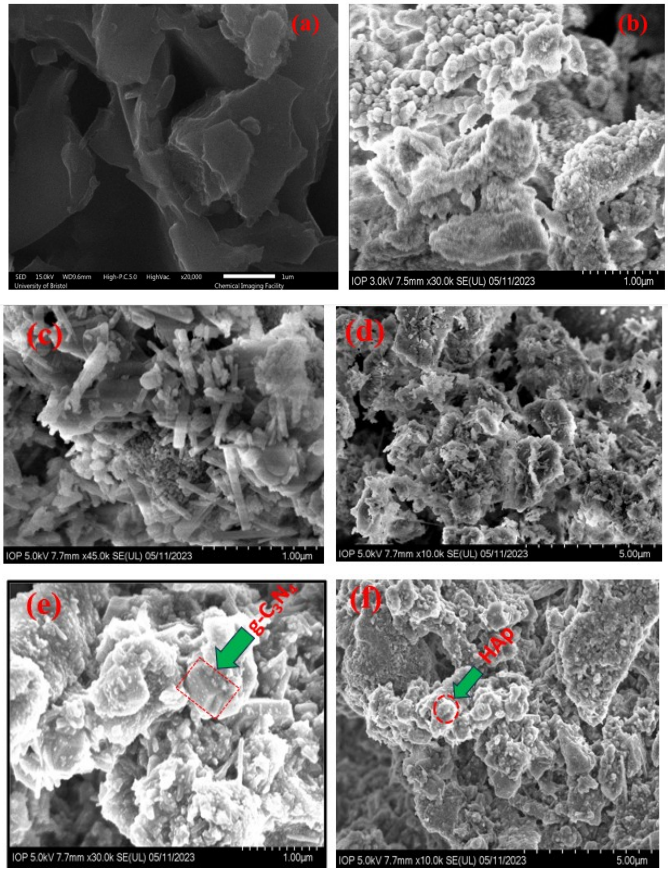

Figure 3. SEM images of (a) g-C_3N_4, (b) HAp, (c, d) g-C_3N_4@HAp and (e, f) Ag-g-C_3N_4@HAp.

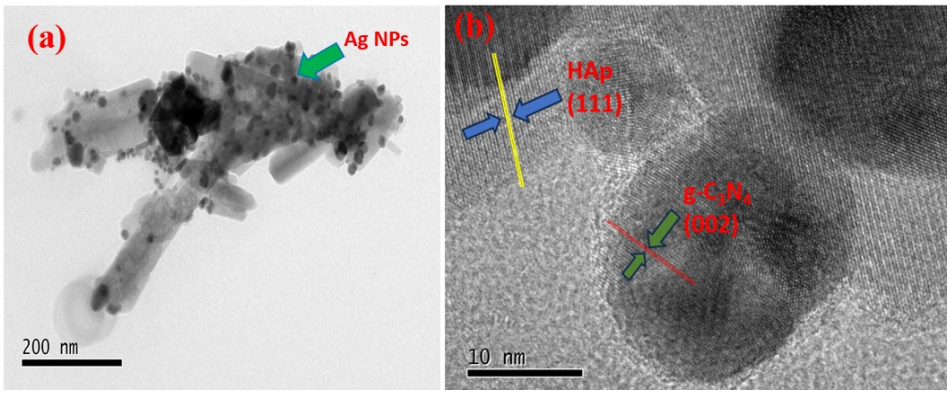

Figure 4. TEM image of Ag-g-C_3N_4@HAp.

SEM images (Figures 3(e), (f)) and TEM images of Ag-g-C_3N_4@HAp (Figure 4) display the size distribution of Ag nanoparticles dispersed on g-C_3N_4@HAp composite (Figure 4(a)) and the lattice spacing of the (111) and (002) plane of nHAp and g-C_3N_4, respectively.

The XPS spectra were used to determine the chemical composition and valence states of Ag-g-C_3N_4@HAp composite. It can also be seen from Figure 5(a) that there are the peaks of C, N, O, Ca and Ag of sample.

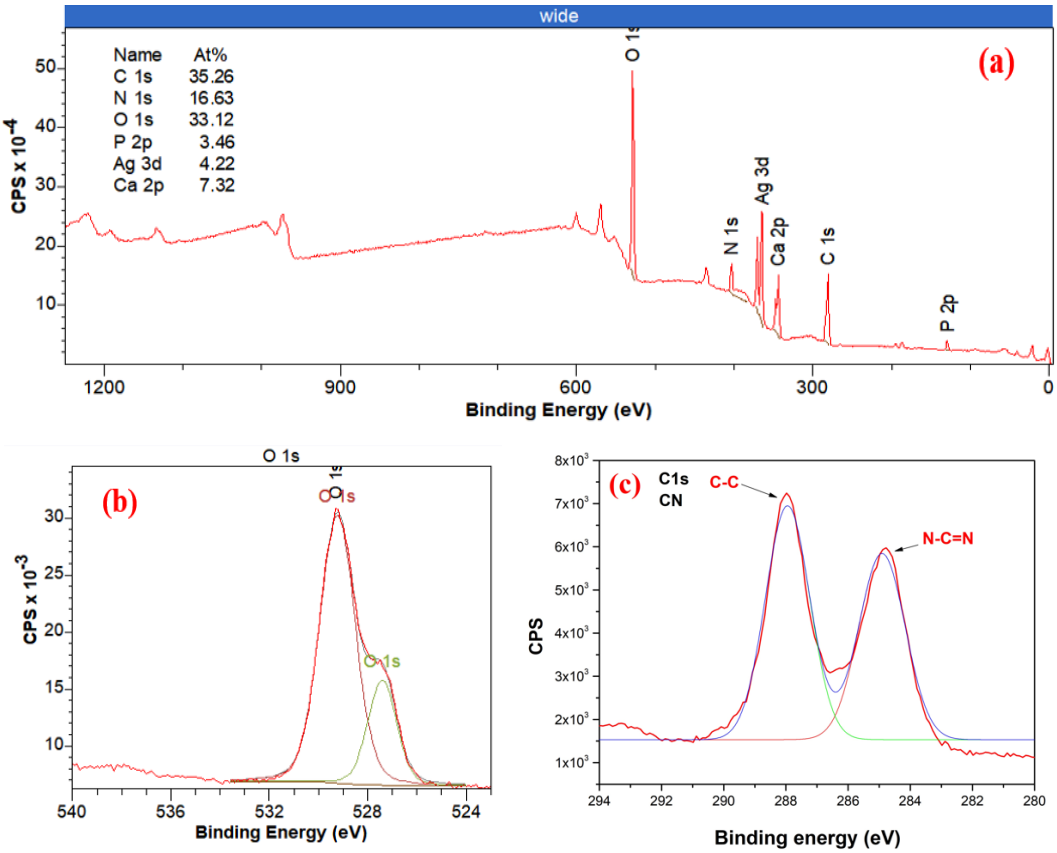

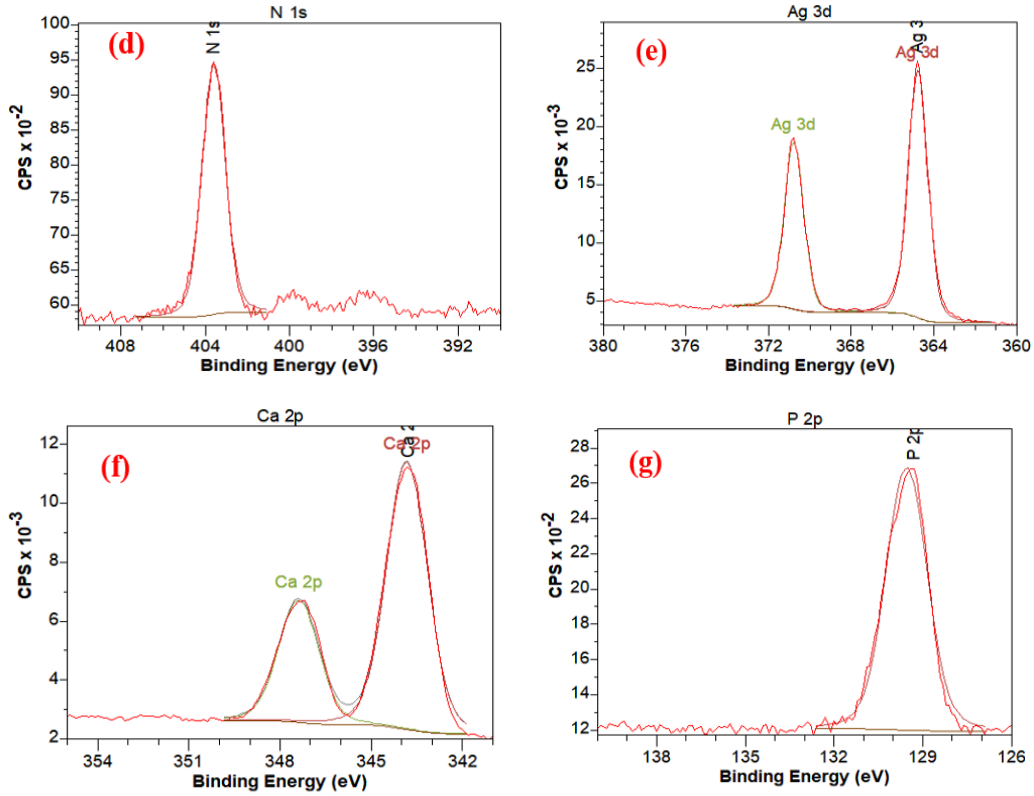

Figure 5. XPS spectra of Ag-g-C_3N_4@HAp: (a) survey spectrum, (b) O 1s, (c) C 1s, (d) N 1s, (e) Ag 3d, (f) Ca 2p, and (g) P 2p.

The high resolution spectra of C 1s (Figure 5(c)) shows three peaks at about 284.6 and 288.1 eV, which were assigned to the C–C, N–C=N bonds of graphitic carbon and sp^2–bonded carbon atoms. As shown in Figure 5(d), peaks of N 1s located at 396.8, 400.1 and 403.6 eV can be assigned as the sp^2–bonded nitrogen in C−N=C groups, sp^3-tertiary nitrogen N−$(C)_3$ and C−N−H of the amino functional groups, respectively [32]. Besides, the O 1s peak (Figure 5(b)) in the range of the binding energy of 529–530 eV, indicating the lattice oxygen (O^{2-}) [33]. The Ca $2p_{3/2}$ binding energies at 347.4 and 344.0 eV (Figure 5(f)) and P $2p_{3/2}$ peak centered at 129.6 eV (Figure 5(g)) were attributed to P−O and O−Ca bonds in structure of HAp [34]. Figure 5(e) shows that Ag 3d spectra could be separated into two peaks centered at about 370.8 and 365.7 eV was assigned as the metallic Ag $3d_{5/2}$ binding energy, namely metallic silver (Ag°) and silver ion (Ag^+) on the surface, respectively [35]. This result is consistent with XRD, TEM analysis, which demonstrated the presence of Ag nanoparticles in the composite.

The optical absorption ability of g-C_3N_4, g-C_3N_4@HAp and Ag-g-C_3N_4@HAp composites were determined through UV-vis spectroscopy and the results are shown in Figure 6.

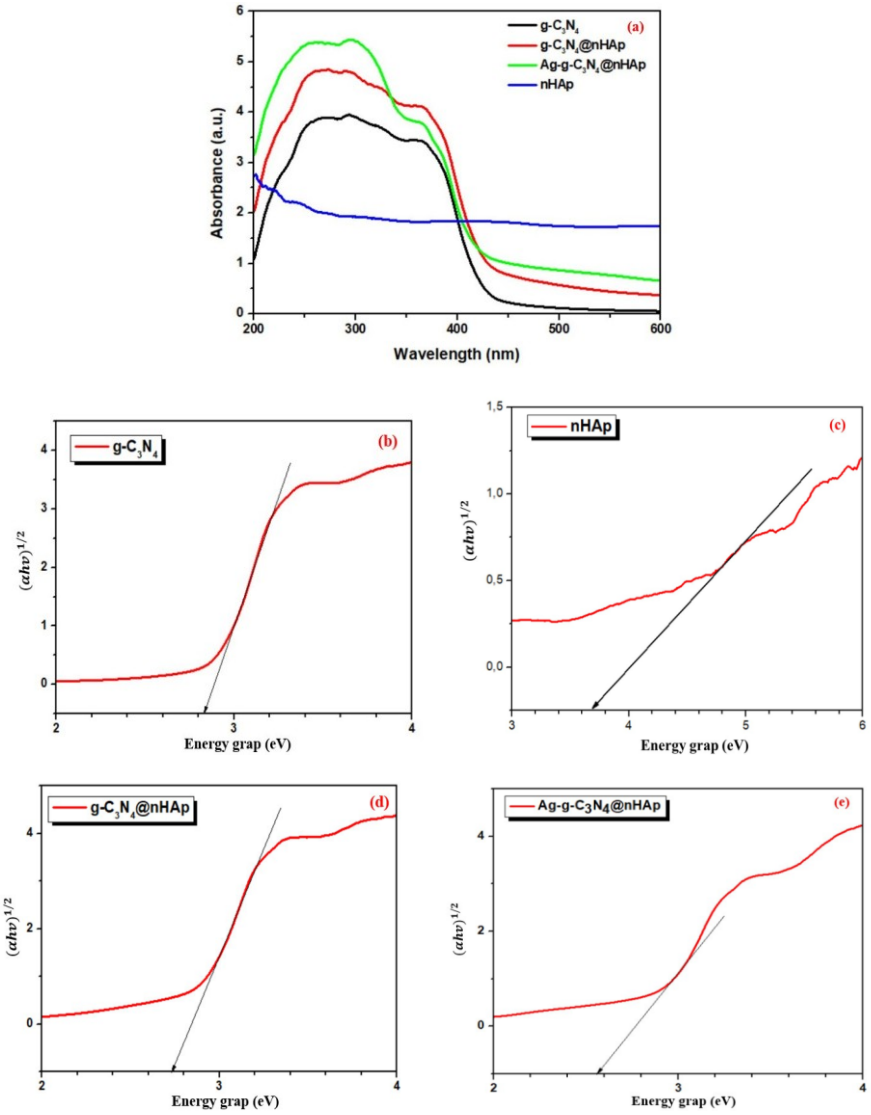

Figure 6. (a) UV-vis spectra; and energy bandgap of: (b) g-C_3N_4, (c) g-C_3N_4@nHAp, (d) Ag-g-C_3N_4@nHAp composite.

Obviously, the absorption of HAp in the ultraviolet light region is weak. The light absorption of g-C_3N_4 is observed at wavelength of 470 nm, while the light absorption is stronger and broader in both visible and ultraviolet for g-C_3N_4@HAp and Ag-g-C_3N_4@HAp composite. Furthermore, the Ag-g-C_3N_4@HAp showed an increase in absorption intensity when silver nanoparticles are composited into the g-C_3N_4@HAp. Band gap energies of the samples were calculated using Tauc plot and the results are shown in Figures 6(b), (c), (d) and (e). The band gap energy values of HAp, g-C_3N_4, g-C_4N_4@HAp and Ag-g-C_3N_4@HAp composites were 3.7, 2.81, 2.76 and 2.59 eV, respectively. The decrease in band gap energy for the composite samples is due to the strong interaction between HAp and g-C_3N_4 layers. The Ag-g-C_3N_4@HAp composite showed a similar light absorption range with g-C_3N_4@HAp composite, but the visible light absorption increased as evidenced in Figure 6(a), which may be due to surface plasma resonance (SPR) effect of silver nanoparticles [36]. The enhanced light absorption indicates that the photoexcited electrons are

easily transferred from valence band (VB) to the conduction band (CB) to generate photogenerated electrons and holes to increase the photocatalytic efficiency.

3.2. Photocatalytic degradation of tetracycline

The photocatalytic degradation ability of nHAp, g-C_3N_4@HAp and Ag-g-C_3N_4@HAp was investigated for TC conversion under visible light irradiation and the results are shown in Figure 7(a). As seen, all synthesized samples showed about 50 % TC adsorption within 30 minutes under dark condition. For pure HAp, during 60 min of visible light illumination, the TC degradation reached 90 % and the conversion remained unchanged during 120 minutes of illumination. Meanwhile, the degradation efficiency of TC using g-C_3N_4@HAp and Ag-g-C_3N_4@HAp composites were 96 % and 99.5 %, respectively, after 120 minutes exposed under visible light irradiation. Regarding the photocatalysts, the Ag-g-C_3N_4@HAp has the highest photocatalytic activity, so that nearly 100 % TC was degraded within 120 min, which was due to the enhanced separation efficiency of photogenerated electron-hole pairs at the interface and surface plasma effect of silver nanoparticles [37]. Besides, the incorporation of Ag nanoparticles limited the photogenerated electron-hole recombination of composite sample. For pure nHAp, in addition to its adsorption capacity, this material also has photocatalytic activity [38], specifically, HAp removes TC up to 90 %.

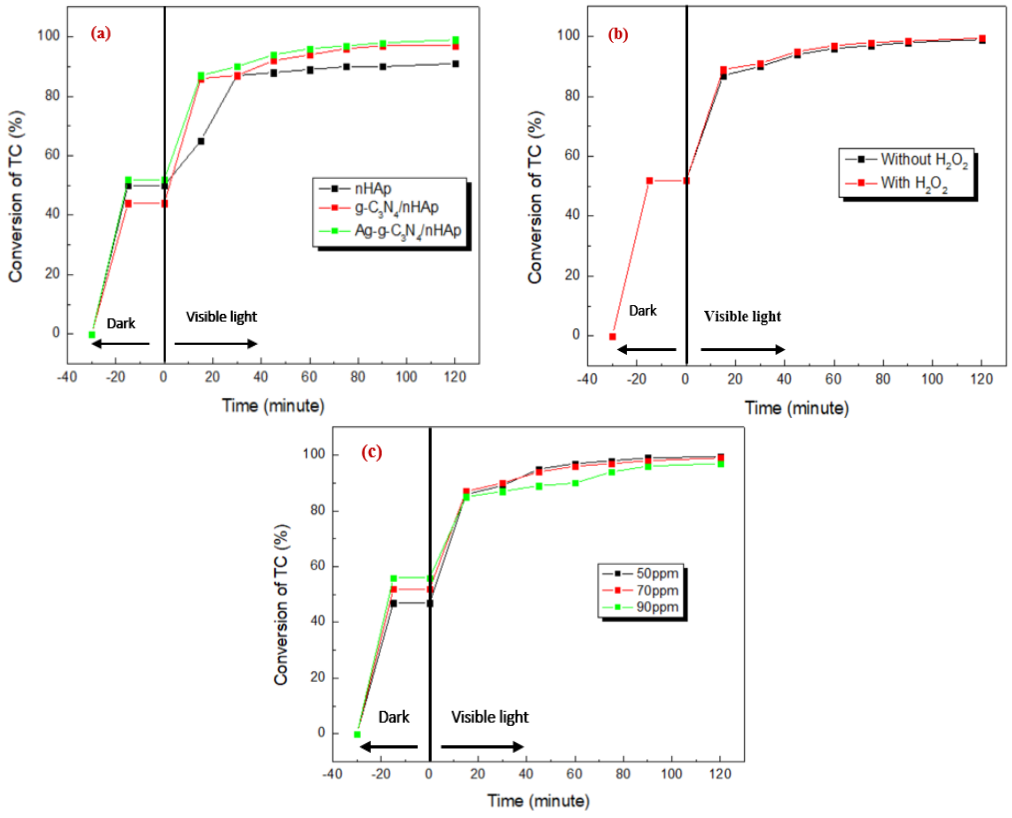

Figure 7. Photodegradation of TC: (a) using nHAp, g-C_3N_4@HAp and Ag-g-C_3N_4@HAp; (b) with H_2O_2 and without H_2O_2 using Ag-g- C_3N_4@HAp; and (c) different concentration of TC using Ag-g- C_3N_4@HAp. (Reaction conditions: 40 mg of photocatalyst, 50 mL of sample solution, visible light, room temperature).

Figure 7(b) shows the photocatalytic degradation of TC using Ag-g-C_3N_4@HAp composite with H_2O_2 used as the oxidizing agent. The results show that in both with and without H_2O_2, TC degradation almost completes after 120 min. Thus, using the Ag-g-C_3N_4@HAp composite as photocatalyst inhibited the recombination process e^-/h^+ and increased the efficiency of free radical generation in the TC degradation process.

The effect of TC concentration was also investigated with Ag-g-C_3N_4@HAp catalyst (Figure 7(c)). The results showed that when increasing the TC concentration from 50 ppm to 90 ppm, the photodegradation efficiency decreased from 99.5 % to 96 %. This may be due to the decreased interaction between TC reactant molecules and catalytic active sites. Table 1 shows photodegradation of TC over various HAp-based photocatalyst composites.

Table 1. Comparative photocatalytic efficiency of various HAp-based photocatalyst composites used for the removal of TC.

Catalyst	Degradation (%)	Experimental conditions				Reference
		Concentration (mg/L)	Volume (mL)	Time (min)	Catalyst dosage (mg)	
g-C_3N_4 (1.5 wt.%)/HAp	100	50	100	15	100	[21]
HARCP@HAp	99.6	50	50	10	Not shown	[39]
CdS (10 wt.%)/HAp	90.2	50	100	30	50	[40]
RP (5.0 wt.%)/HAp	100	10	100	10	100	[41]
Ag-g-C_3N_4@HAp	100	50	50	120	40	This work

When compared with other previously reported HAp-based photocatalyst composites for photocatalytic removal of TC, as shown in Table 1, the Ag-g-g-C_3N_4@HAp used in this study clearly showed similar photocatalytic activity. More important, the green photocatalyst of Ag-g-C_3N_4@HAp composite has been synthesized from naturally available, environmentally friendly materials. Therefore, the Ag-g-C_3N_4@HAp composite can be considered a green photocatalyst in applications for antibiotics decomposition in water environment.

4. CONCLUSION

A novel composite of Ag-g-C_3N_4@HAp has been successfully synthesized using natural raw materials as seashells and *Centella asiatica* (L.) Urban extract. The photocatalytic effect of the composite was used to degrade TC in aqueous solution. The photocatalytic efficiency has been improved when silver nanoparticles were dispersed on the g-C_3N_4@HAp substrate, leading to almost completely degradation (99.5 %) after reaction time of 120 min under visible light irradiation. This research has the potential to use available, low-cost raw materials for synthesis of green composites and its application to treat persistent organic molecules in industrial wastewater.

Acknowledgments. This research is funded by Young Talent Fund for Student of Hanoi University of Mining and Geology.

CRediT authorship contribution statement. Pham Xuan Nui: Conceptualization, Methodology, Supervision, Writing – review & editing. Pham Thi Yen Phi: Formal analysis, Investigation, Writing – original draft. Phan Trung Kien: Data curation, Formal analysis, Investigation.

Declaration of competing interest. The authors declare that they have no known competing financial interests or personal relationships that could have appeared to influence the work reported in this paper.

REFERENCES

1. Fattahimoghaddam H., Mahvelati-Shamsabadi T., Lee B. K. - Efficient photodegradation of rhodamine B and tetracycline over robust and green g-C_3N_4 nanostructures: supramolecular design. J. Hazard. Mater., **403** (2021) 123703. https://doi.org/10.1016/j.jhazmat.2020.123703.
2. Raizada P., Kumar A., Singh P. - Graphitic carbon nitride-based new advanced materials for photocatalytic applications. Curr. Anal. Chem., **17**(2) (2021) 150-165. https://doi.org/10.2174/15734110MTAz0MzMFy.
3. Qi K., Liu S., Zada A. - Graphitic carbon nitride, a polymer photocatalyst. J. Taiwan Inst. Chem. Eng., **109** (2020) 111-123. https://doi.org/10.1016/j.jtice.2020.02.012.
4. Reddy K. R., Reddy C. H. V., Nadagouda M. N., Shetti N. P., Jaesool S., Aminabhavi T. M. - Polymeric graphitic carbon nitride (g-C_3N_4)-based semiconducting nanostructured materials: synthesis methods, properties and photocatalytic applications. J. Environ. Manag., **238** (2019) 25-40. https://doi.org/10.1016/j.jenvman.2019.02.075.
5. Naseri A., Samadi M., Pourjavadi A., Moshfegh A. Z., Ramakrishna S. - Graphitic carbon nitride (g-C_3N_4)-based photocatalysts for solar hydrogen generation: recent advances and future development directions. J. Mater. Chem. A, **5**(45) (2017) 23406-23433. https://doi.org/10.1039/C7TA05131J.
6. Wen J., Xie J., Chen X., Li X. - A review on g-C_3N_4-based photocatalysts. Appl. Surf. Sci., **391** (2017) 72-123. https://doi.org/10.1016/j.apsusc.2016.07.030.
7. Tong T., Zhu B., Jiang C., Cheng B., Yu J. - Mechanistic insight into the enhanced photocatalytic activity of single-atom Pt, Pd or Au-embedded g-C_3N_4. Appl. Surf. Sci., **433** (2018) 1175-1183. https://doi.org/10.1016/j.apsusc.2017.10.120.
8. Patnaik S., Sahoo D. P., Parida K. - An overview on Ag modified g-C_3N_4 based nanostructured materials for energy and environmental applications. Renew. Sustain. Energy Rev., **82** (2018) 1297-1312. https://doi.org/10.1016/j.rser.2017.09.026.
9. Bu Y., Chen Z., Li W. - Using electrochemical methods to study the promotion mechanism of the photoelectric conversion performance of Ag-modified mesoporous g-C_3N_4 heterojunction material. Appl. Catal., B, **144** (2014) 622-630. https://doi.org/10.1016/j.apcatb.2013.07.066.
10. Fu Y., Huang T., Zhang L., Zhu J., Wang X. - Ag/g-C_3N_4 catalyst with superior catalytic performance for the degradation of dyes: a borohydride-generated superoxide radical approach. Nanoscale, **7**(32) (2015) 13723-13733. https://doi.org/10.1039/C5NR03260A.
11. Bürger C., Fischer D. R., Cordenunzzi D. A., de Borba Batschauer A. P., Filho V. C., dos Santos Soares A. R. - Acute and subacute toxicity of the hydroalcoholic extract from *Wedelia paludosa* (*Acmela brasiliensis*) (Asteracea) in mice. J. Pharm. Sci., **8**(2) (2015) 370-373.
12. Au H. T., Pham L. N., Vu T. H. T., Park J. S. - Fabrication of an antibacterial non-woven mat of a poly (lactic acid)/chitosan blend by electrospinning. Macromol. Res., **20**(1) (2011) 51-58. https://doi.org/10.1007/s13233-012-0010-9.
13. Das R. K., Borthakur B. B., Bora U. - Green synthesis of gold nanoparticles using ethanolic leaf extract of *Centella asiatica*. Mater. Lett., **64**(13) (2010) 1445-1447. https://doi.org/10.1016/j.matlet.2010.03.051.
14. Fina F., Ménard H., Irvine J. T. S. - The effect of Pt NPs crystallinity and distribution on the photocatalytic activity of Pt-g-C_3N_4. Phys. Chem. Chem. Phys., **17**(21) (2015) 13929-13936. https://doi.org/10.1039/C5CP00560D.
15. Manimozhi R., Mathankumar M., Gnana Prakash A. P. - Synthesis of g-C_3N_4/ZnO heterostructure photocatalyst for enhanced visible degradation of organic dye. Optik, **229** (2021) 165548. https://doi.org/10.1016/j.ijleo.2020.165548.
16. Phan T. S., Sane A. R., Rêgo de Vasconcelos B., Nzihou A., Sharrock P., Grouset D., Pham Minh D. - Hydroxyapatite supported bimetallic cobalt and nickel catalysts for syngas production from dry reforming of methane. Appl. Catal. B Environ., **224** (2018) 310-321. https://doi.org/10.1016/j.apcatb.2017.10.063.

17. Reddy M., Venugopal A., Subrahmanyam M. - Hydroxyapatite photocatalytic degradation of calmagite (an azo dye) in aqueous suspension. Appl. Catal. B: Environ., **69**(3-4) (2007) 164-170. https://doi.org/10.1016/j.apcatb.2006.07.003.
18. Kojima S., Nagata F., Kugimiya S., Kato K. - Synthesis of peptide-containing calcium phosphate nanoparticles exhibiting highly selective adsorption of various proteins. Appl. Surf. Sci., **458** (2018) 438-445. https://doi.org/10.1016/j.apsusc.2018.07.114.
19. Wang X., Zhang L., Zeng Q., Jiang G., Yang M. - First-principles study on the hydroxyl migration from inner to surface in hydroxyapatite. Appl. Surf. Sci., **452** (2018) 381-388. https://doi.org/10.1016/j.apsusc.2018.05.050.
20. Jiang R., Liu M., Huang H., Huang L., Huang Q., Wen Y., Cao Q. y., Tian J., Zhang X., Wei Y. - A novel self-catalyzed photoATRP strategy for preparation of fluorescent hydroxyapatite nanoparticles and their biological imaging. Appl. Surf. Sci., **434** (2018) 1129-1136. https://doi.org/10.1016/j.apsusc.2017.11.039.
21. Prakash M., Lemaire T., Di Tommaso D., de Leeuw N., Lewerenz M., Caruel M., Naili S. - Transport properties of water molecules confined between hydroxyapaptite surfaces: A Molecular dynamics simulation approach. Appl. Surf. Sci., **418** (2017) 296-301. https://doi.org/10.1016/j.apsusc.2017.02.029.
22. Dileep Kumar V. G., Sridhar M. S., Aramwit P., Krut'ko V. K., Musskaya O. N., Glazov I. E., Reddy N. - A review on the synthesis and properties of hydroxyapatite for biomedical applications. J. Biomater. Sci. Polym. Ed., **33**(2) (2022) 229-261. https://doi.org/10.1080/09205063.2021.1980985.
23. Nishikawa H. - Surface changes and radical formation on hydroxyapatite by UV irradiation for inducing photocatalytic activation. J. Mol. Catal. A Chem., **206**(1-2) (2003) 331-338. https://doi.org/10.1016/S1381-1169(03)00414-X.
24. Xu T., Zou R., Lei X., Qi X., Wu Q., Yao W., Xu Q. - New and stable g-C_3N_4/HAp composites as highly efficient photocatalysts for tetracycline fast degradation. Appl. Catal. B Environ., **245** (2019) 662-671. https://doi.org/10.1016/j.apcatb.2019.01.020.
25. Ehiro T. - Application of a calcined animal bone to synthesis of graphitic carbon nitride composite. Environ. Technol., **43**(10) (2022) 1573-1582. https://doi.org/10.1080/09593330.2020.1841833.
26. Jiménez-Flores Y., Jiménez-Rangel K., Samaniego-Benítez J. E., Lartundo-Rojas L., Calderón H. A., Gómez R., Mantilla A. - Novelty g-C_3N_4/HAp composite as highly effective photocatalyst for Cr (VI) photoreduction. Catal. Today, **388-389** (2022) 168-175. https://doi.org/10.1016/j.cattod.2020.07.045.
27. Beygli R. A., Mohaghegh N., Rahimi E. - Metal ion adsorption from wastewater by g-C_3N_4 modified with hydroxyapatite: a case study from Sarcheshmeh Acid Mine Drainage. Res. Chem. Intermed., **45**(4) (2019) 2255-2268. https://doi.org/10.1007/s11164-018-03733-9.
28. Nguyen H. T., Doan H. V., Nguyen T. T. B., Pham X. N. - Nanoarchitectonics of Ag-modified g-C_3N_4@halloysite nanotubes by a green method for enhanced photocatalytic efficiency. Adv. Powder Technol., **33**(12) (2022) 103862. https://doi.org/10.1016/j.apt.2022.103862.
29. Pham X. N., Nguyen H. T., Pham N. T. - Green Synthesis and Antibacterial Activity of HAp@Ag Nanocomposite Using *Centella asiatica* (L.) Urban Extract and Eggshell. Int. J. Biomater., **2020** (2020) 8841221. https://doi.org/10.1155/2020/8841221.
30. Zhang R., Zhang X., Liu S., Tong J., Kong F., Sun N., Han X., Zhang Y. - Enhanced photocatalytic activity and optical response mechanism of porous graphitic carbon nitride (g-C_3N_4) nanosheets. Mater. Res. Bull., **140** (2021) 111263. https://doi.org/10.1016/j.materresbull.2021.111263.
31. Liu R., Yang W., He G., Zheng W., Li M., Tao W., Tian M. - Ag-Modified g-C_3N_4 prepared by a one-step calcination method for enhanced catalytic efficiency and stability. ACS Omega, **5**(31) (2020) 19615-19624. https://doi.org/10.1021/acsomega.0c02161.
32. Qi K., Xie Y., Wang R., Liu S. y., Zhao Z. - Electroless plating Ni-P cocatalyst decorated g-C_3N_4 with enhanced photocatalytic water splitting for H_2 generation. Appl. Surf. Sci., **466** (2019) 847-853. https://doi.org/10.1016/j.apsusc.2018.10.037.
33. Hou Z., Feng J., Lin T., Zhang H., Zhou X., Chen Y. - The performance of manganese-based catalysts with $Ce_{0.65}Zr_{0.35}O_2$ as support for catalytic oxidation of toluene. Appl. Surf. Sci., **434** (2018) 82-90. https://doi.org/10.1016/j.apsusc.2017.09.048.

34. López E. O., Bernardo P. L., Checca N. R., Rossi A. L., Mello A., Ellis D. E., Rossi A. M., Terra J. - Hydroxyapatite and lead-substituted hydroxyapatite near-surface structures: Novel modelling of photoemission lines from X-ray photoelectron spectra. Appl. Surf. Sci., **571** (2022) 151310. https://doi.org/10.1016/j.apsusc.2021.151310.
35. Tian K., Liu W. J., Jiang H. - Comparative investigation on photoreactivity and mechanism of biogenic and chemosynthetic Ag/C_3N_4 composites under visible light irradiation. ACS Sustain. Chem. Eng., **3**(2) (2015) 269-276. https://doi.org/10.1021/sc500646a.
36. Pham X. N., Nguyen M. B., Ngo H. S., Doan H. V. - Highly efficient photocatalytic oxidative desulfurization of dibenzothiophene with sunlight irradiation using green catalyst of Ag@AgBr/Al-SBA-15 derived from natural halloysite. J. Ind. Eng. Chem., **90** (2020) 358-370. https://doi.org/10.1016/j.jiec.2020.07.037.
37. Duan S., Ai Y. J., Hu W., Liu Y. - Roles of plasmonic excitation and protonation on photoreactions of p-Aminobenzenethiol on Ag nanoparticles. J. Phys. Chem. C, **118**(13) (2014) 6893-6902. https://doi.org/10.1021/jp500728s.
38. Márquez Brazón E., Piccirillo C., Moreira I. S., Castro P. M. L. - Photodegradation of pharmaceutical persistent pollutants using hydroxyapatite-based materials. J. Environ. Manage., **182** (2016) 486-495. https://doi.org/10.1016/j.jenvman.2016.08.005.
39. Lu L., Zhang Y., Yang Z., Xu J., Li M., Wang Y., Wang L., Huang S., Ren Y. - Easily fabricated HARCP/HAp photocatalyst for efficient and fast removal of tetracycline under natural sunlight. Chem. Eng. J., **412** (2021) 128620. https://doi.org/10.1016/j.cej.2021.128620.
40. Lei X., Xu T., Yao W., Wu Q., Zou R. - Hollow hydroxyapatite microspheres modified by CdS nanoparticles for efficiently photocatalytic degradation of tetracycline. J. Taiwan Inst. Chem. Eng., **106** (2020) 148-158. https://doi.org/10.1016/j.jtice.2019.10.023.
41. Zou R., Xu T., Lei X., Wu Q., Xue S. - Novel and efficient red phosphorus/hollow hydroxyapatite microsphere photocatalyst for fast removal of antibiotic pollutants. J. Phys. Chem. Solids, **139** (2020) 109353. https://doi.org/10.1016/j.jpcs.2020.109353.